CO2 emission estimation in the urban environment: measurement of the CO2 storage term

Atmospheric Environment 122 (2015) 775–790

Contents lists available at ScienceDirect

Atmospheric Environment

journal homepage: www.elsevier.com/locate/atmosenv

CO_2 emission estimation in the urban environment: Measurement of the CO_2 storage term

A.B. Bjorkegren [a, *], C.S.B. Grimmond [b, a, **], S. Kotthaus [a, b], B.D. Malamud [a]

[a] Department of Geography, King's College London, London, WC2R 2LS, UK
[b] Department of Meteorology, University of Reading, Reading, RG6 6BB, UK

HIGHLIGHTS

- Diurnal and seasonal CO_2 storage (ΔC_S) cycles in an urban street canyon reported.
- Effect of sensor position, sampling rate, and data processing on ΔC_S assessed.
- Method of calculating ΔC_S from measurements at one height shown to be invalid.
- Spectral analysis of ΔC_S suggests an inverse power law relationship with frequency.
- Storage and vertical flux compared across a full seasonal cycle.

ARTICLE INFO

Article history:
Received 6 March 2015
Received in revised form
5 October 2015
Accepted 6 October 2015
Available online 19 October 2015

Keywords:
Carbon dioxide
Wavelet analysis
CO_2 storage
Urban environment
CO_2 profile

ABSTRACT

Eddy covariance has been used in urban areas to evaluate the net exchange of CO_2 between the surface and the atmosphere. Typically, only the vertical flux is measured at a height 2–3 times that of the local roughness elements; however, under conditions of relatively low instability, CO_2 may accumulate in the airspace below the measurement height. This can result in inaccurate emissions estimates if the accumulated CO_2 drains away or is flushed upwards during thermal expansion of the boundary layer. Some studies apply a single height storage correction; however, this requires the assumption that the response of the CO_2 concentration profile to forcing is constant with height. Here a full seasonal cycle (7th June 2012 to 3rd June 2013) of single height CO_2 storage data calculated from concentrations measured at 10 Hz by open path gas analyser are compared to a data set calculated from a concurrent switched vertical profile measured (2 Hz, closed path gas analyser) at 10 heights within and above a street canyon in central London. The assumption required for the former storage determination is shown to be invalid. For approximately regular street canyons at least one other measurement is required. Continuous measurements at fewer locations are shown to be preferable to a spatially dense, switched profile, as temporal interpolation is ineffective. The majority of the spectral energy of the CO_2 storage time series was found to be between 0.001 and 0.2 Hz (500 and 5 s respectively); however, sampling frequencies of 2 Hz and below still result in significantly lower CO_2 storage values. An empirical method of correcting CO_2 storage values from under-sampled time series is proposed.

1. Introduction

Human activity in urban areas is responsible for 30–40% of directly emitted anthropogenic greenhouse gases (Satterthwaite, 2008) and 70% of total emissions of CO_2 (Canadell et al., 2009). Several urban studies have assessed net emissions at the local scale (10^2–10^4 m) using the eddy covariance (EC) method (Grimmond and Christen, 2012; Christen, 2014). Here net ecosystem exchange (NEE) is calculated as the sum of the CO_2 exchanges through the sides of a notional volume of air and the change in the amount of CO_2 stored (ΔC_S) within the volume (Aubinet et al., 2005). In practice, many monitoring sites (Grimmond et al., 2002; Baldocchi, 2003; Velasco and Roth, 2010) approximate NEE as the net flux into or out of the top of the volume of interest, assuming horizontal homogeneity (horizontal advection into the volume is equal to

* Corresponding author.
** Corresponding author.
E-mail addresses: alex.bjorkegren@kcl.ac.uk (A.B. Bjorkegren), c.s.grimmond@reading.ac.uk (C.S.B. Grimmond).

http://dx.doi.org/10.1016/j.atmosenv.2015.10.012

transport out of the volume) and fully turbulent conditions with negligible storage. In urban environments during stable atmospheric conditions the ΔC_S term will be non-negligible (Helfter et al., 2011); for example, ΔC_S was found to be five times the magnitude of the turbulent vertical flux term (F_{CO2}) close to dawn and dusk in suburban Vancouver, Canada (Crawford and Christen, 2014). Other urban studies found ΔC_S to be smaller, but still significant, with maximum ΔC_S values 11% and 22% of the magnitude of F_{CO2} in Edinburgh, Scotland (Nemitz et al. 2002) and Basel, Switzerland (Feigenwinter et al. 2012), respectively. Similarly, in rural environments horizontal advection may be non-negligible (e.g., Aubinet et al., 2003). This paper focuses on the methodological considerations when assessing ΔC_S from a vertical profile in an urban environment. Future manuscripts will address horizontal variation and advection.

Of three studies discussed above (Vancouver, Edinburgh, Basel) with reported urban CO_2 storage values, only one (Vancouver, Crawford and Christen, 2014) presented values derived from a dataset of longer than one month; however, both these values and those reported for Edinburgh by Nemitz et al. (2002) were calculated based on the assumption of a constant relation between carbon dioxide concentration ($[CO_2]$) measured above the blending height and the concentration in the street canyon. In contrast, for Basel, Feigenwinter et al. (2012) did not make this assumption and reported ΔC_S calculated from $[CO_2]$ at ten levels; however, the results are only for one month (15th June to 15th July 2002). There is therefore scope to improve not only the understanding of the processes affecting CO_2 storage over a greater range of meteorological and anthropogenic conditions, but also to develop recommendations for future measurement programmes.

The objective of this paper is to evaluate potential approaches for such studies, illustrated with examples from, and analysis of, high temporal resolution data collected at 10 locations from 6.5 to 46.4 m above ground level between 2011 and 2014 at King's College London, in Central London, UK. The paper is organized as follows. In the rest of this Section 1 we provide a brief background of how CO_2 storage is calculated and then (Section 2) a discussion of the methods used in this paper. This is followed by an exploration of the temporal variation of CO_2 storage (Section 3) and the relation between measured CO_2 storage and anthropogenic and natural factors in a highly urbanised environment (Section 4). The required number and placement of sample points for CO_2 storage measurements in a deep urban street canyon is addressed (Section 5) and the effect of sensor response and sampling interval on calculated CO_2 storage is tested (Section 6). At the processing stage, three different temporal and spatial interpolation methods are evaluated against measured data (Section 7). Finally, the impact of CO_2 storage calculated by two different methods on the turbulent vertical CO_2 flux is assessed. The Supplementary material (noted by S.1 to S.9), includes the notation with corresponding units (S.1) used in the text, further information on CO_2 storage calculation (S.2), previous CO_2 storage studies (S.3), equipment (S.4), meteorological characteristics (S.5), example time series (S.6), variations of CO_2 with friction velocity, wind direction and height above ground level (S.7, S.8) and further references (S.9). The online version of this paper provides the figures in colour.

1.1. Calculation of CO_2 storage

There are two main approaches to calculating CO_2 storage flux density, i.e., the rate of change of CO_2 per unit area below the Eddy Covariance (EC) measurement height. Here they are referred to as the 'single height' and the 'profile' approaches. For a brief discussion of the theory and some reported results, see Supplementary material S.2 and S.3, respectively. For a more in depth discussion of the theoretical considerations regarding CO_2 storage the reader is referred to Finnigan (2006) and subsequent discussion (Kowalksi, 2008; Finnigan, 2009).

The approach to calculate CO_2 storage depends upon the number of vertical locations at which CO_2 concentration ($[CO_2]$, the symbol $[\ ]$ is used to indicate concentration) data are collected. In the first approach, 'single height' CO_2 storage (ΔC_{SS}) is calculated from $[CO_2]$ data at one location, usually by eddy covariance equipment in the inertial sub-layer (Nemitz et al., 2002; Crawford and Christen, 2014). In the second approach, the 'profile' method, ΔC_S is calculated from data collected at multiple heights (ΔC_{SP}). The profile method uses a vertical $[CO_2]$ profile at heights z_i, which is generally measured by cycling through all the sample locations within a set time period with a data-logger controlled valve array (Xu et al., 1999; Mölder et al., 2000; Vogt et al., 2006; Hutyra et al., 2008). This cycle period may not be the same as the averaging period used in the ΔC_{SP} calculation. For example, measurements collected with a sampling interval, t_s, of 2 Hz for 75 s at 8 heights, giving a full profile cycle every 10 min, may be used to calculate ΔC_{SP} with an averaging period (T) of 30 min. The storage is calculated as the sum of the changes in time averaged concentration ($\overline{[CO_2]}_i$) between time $t = -T/2$ and $t = T/2$ for each location (i) in the profile, weighted by the vertical span, Δz_i, over which each profile measurement is considered to be representative and divided by the averaging period (T), which can be expressed as (modified from Aubinet et al., 2005):

$$\Delta C_{SP} = \frac{1}{T}\sum_i \left(\overline{[CO_2]}_{i,\ t=\frac{T}{2}} - \overline{[CO_2]}_{i,\ t=-\frac{T}{2}}\right)\Delta z_i \quad (1)$$

If the measurements at each height are not made concurrently, $[CO_2]$ at each height may first be interpolated in time to generate instantaneous profiles from which ΔC_{SP} can be calculated, though this is neglected in some cases (Iwata et al., 2005). The impact of interpolation on calculated ΔC_{SP} is discussed further in Section 7.

The single height method is a simplification of the profile method to one height, which is usually the height of the eddy covariance equipment. The change in $[CO_2]$ with time at z_h ($\Delta[CO_2]/\Delta t$) is weighted by the vertical distance from the ground to the measurement point (z_h). The single height CO_2 storage (ΔC_{SS}) is given by (modified from Nemitz et al., 2002):

$$\Delta C_{SS} = \frac{\Delta[CO_2]}{\Delta t} z_h \quad (2)$$

As the data are continuous, the change in the instantaneous CO_2 concentration with time ($\Delta[CO_2]/\Delta t$) can be used instead of the change in the time averaged CO_2 concentration with time ($\Delta\overline{[CO_2]}/\Delta t$), though it may still be advisable to average in time to reduce measurement noise (Finnigan, 2006).

The ΔC_{SS} calculation assumes any change in $[CO_2]$ below the measurement height results in a change of equivalent magnitude at the measurement height. This assumption appears not to be supported by any evidence in the literature; reported diurnal cycles of CO_2 mixing ratios in the roughness sub-layer over both rural (e.g., Xu et al., 1999) and urban (e.g., Lietzke and Vogt, 2013) surfaces are known to vary with height. This problem is particularly acute during periods of low turbulence, such as at night or during cold weather, where measurements above the surface layer may become decoupled from processes near ground level (Helfter et al., 2011).

If temporal variability is large compared to the spatial variability, the single height method may provide a more accurate measure of storage than the profile method as the maximum data availability at each sample location for the latter may be $1/k$ of the total time

series, where k is the number of heights. Data availability may be improved by installation of multiple gas analysers (Simpson et al., 1998; Siebicke et al., 2010); however, this introduces the problem of ensuring that measurements are comparable between heights. If horizontal variability of $[CO_2]$ is high, measurements made at one particular height in multiple locations may be averaged prior to integration over the vertical extent of the volume of interest (e.g., Crawford and Christen, 2014). In this paper data from both continuous (two heights, $z_i = 20.5$, 46.4 m above the Strand street canyon (hereafter referred to as the Strand canyon) ground level (a.g.l.)) and switched (10 heights, $z_i = 6.5$, 9.5, 12.5, 16.0, 19.5, 32.3, 33.7, 36.0, 39.3, 46.4 m a.g.l.) CO_2 concentration profiles are reported and compared.

2. Methods

2.1. Site

The study area KS (red dot in Fig. 1a) is situated on the Strand, on the north bank of the River Thames in the centre of the Central Activity Zone in London, UK. The Central Activity Zone is the political, financial, retail and cultural 'hub' of London and, to a lesser extent, the UK. It contains nearly 30% of all of London's jobs (GLA, 2008) and is heavily influenced by commuter traffic: 1.16 million people passed through the Central London cordon (Fig. 1a) during the 07:00 to 10:00 BST (British Summer Time, GMT +1, in effect from the last Sunday of March to the last Sunday of October) morning peak period on an average weekday in 2011, with 18% of the journeys made via a motorised vehicle (DfT, 2013). The relatively small nocturnal population results in lower demands for heating compared to residential areas (Velasco and Roth, 2010; Iamarino et al., 2012; Ward et al., 2015).

Sources of CO_2 in the vicinity of KS include rooftop emissions due to burning of natural gas for heating and venting of high-CO_2 air from air conditioning ducts (Fig. 1b, c; see also Kotthaus and Grimmond, 2012). Chamber measurements suggest the river (not shown) is not a significant source and there are no major power stations or other industrial activity nearby. Land cover characteristics for the EC source areas of the KSS tower (40 m to the east of KSSW) are (% plan area): roads (43%), buildings (38%), water (14%), vegetation, including trees, (5%), trees (2%) (Kotthaus and Grimmond, 2014b). The predominantly mature London Plane trees (*Platanus acerifolia*) line the Strand canyon and other major roads nearby. Whilst photosynthetic uptake of CO_2 does occur, it is likely to be an insignificant control on the vertical CO_2 flux or the CO_2 storage within the monitored street canyon. Ward et al. (2015) found the role of vegetation to be negligible at this site. The street canyon is symmetric and ~31 m deep with a smaller (~18 m)

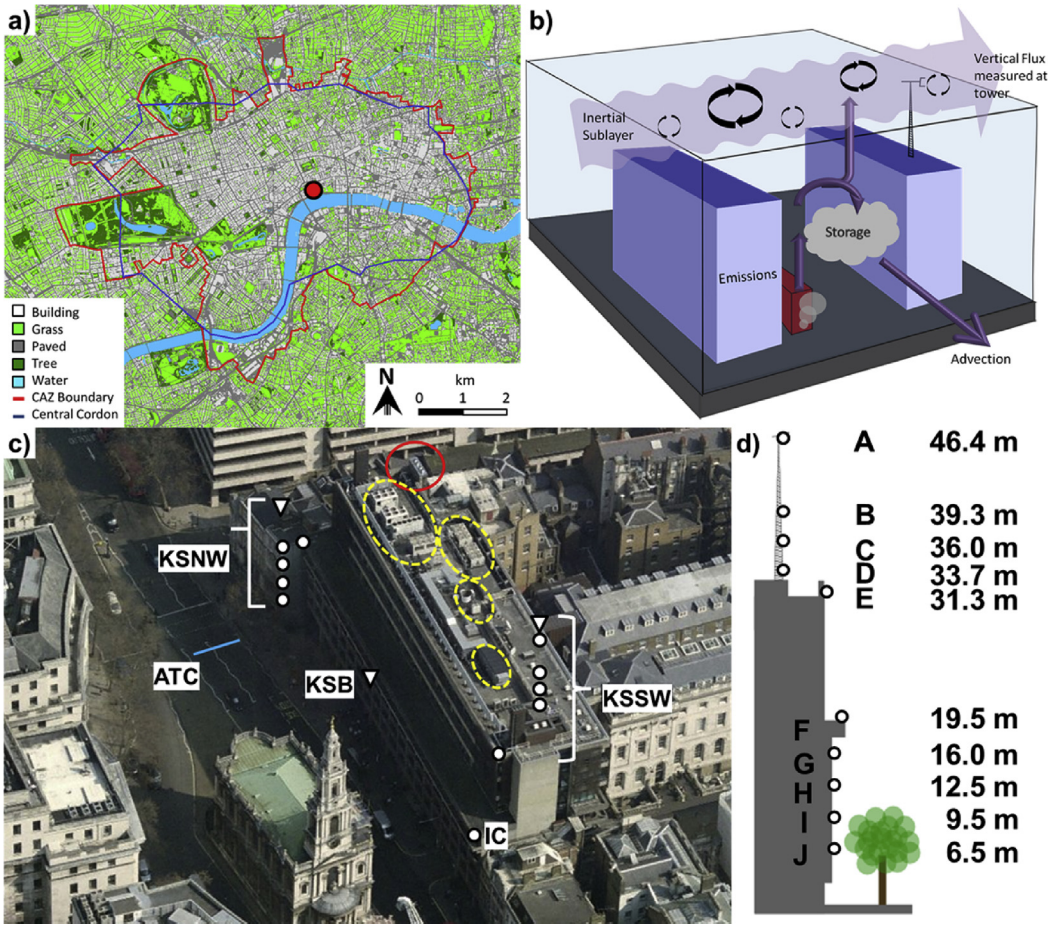

Fig. 1. Sample sites at King's College London, Strand Campus (KS), London, UK. (a) Land cover map (Lindberg and Grimmond, 2011) centred on the Strand campus (red dot) with the Central Activity Zone (CAZ, red line) and Transport for London (TfL) Central London Cordon (blue line). (b) Diagram of a defined volume of air containing two buildings divided by a road, with emissions (e.g., from a bus) stored within the canyon, advected horizontally, or mixed vertically into the inertial sublayer where they may be measured by instruments sited at the top of the volume. (c) Measurement sites at KS include traffic count [undertaken week starting 8th July 2013 (blue line, 'ATC')], switched $[CO_2]$ profile (white circles: KSSW, KSNW and inter comparison point, IC) and EC (white triangles). Rooftop sources are circled: chillers (yellow, dotted), boiler chimneys (red, solid). (d) Vertical $[CO_2]$ profile locations z_i viewed from the ATC location in (c) with height above ground level. Image in (c) taken in October, 2011, during the leaf off period (Microsoft, 2011). (For interpretation of the references to colour in this figure legend, the reader is referred to the web version of this article.).

obstacle (St Mary-le-Strand church, lower left, Fig. 1c) in the centre, which could be considered to form two asymmetric sub-canyons for part of the length of the Strand. The height:width ratio varies from 0.74 to 1.28 with a two-lane, one-way street running east-northeast to west-southwest carrying 16,000–19,000 vehicles (predominantly cars) per day (automated traffic count, Strand, 2013/189 to 196). Throughout this paper we use date format YYYY/DDD = Year/Day of Year. Traffic speed is slow, ranging from a peak average speed of 45 km h^{-1} between 03:00 and 05:00 BST to a minimum of 26 km h^{-1} at the beginning of the evening rush hour peak in traffic volume (18:00 BST). Considerable congestion, particularly in the vicinity of two bus stops (located close to the measurement profile) is observed at this time.

2.2. Equipment and data set

Equipment installed on a guyed tower (13.31 m; T-35H, Aluma Tower Inc., USA) is referred to here as the KSSW site (Fig. 1c). The second site, KSNW (Fig. 1c) consists of a pneumatic mast (<9 m, CSQT9-6/HP, Clark Masts, Belgium) and air inlets for a switched $[CO_2]$ profile on the exterior wall of a building extending down to 6.5 m above street level. Eddy covariance equipment, including fast response open-path infrared gas analysers (LI7500A, LI-COR Biosciences, USA), installed at KSSW and KSNW, have a horizontal separation of 70 m and are 46.4 and 20.5 m above ground level respectively. Note, as measurements are made within the street canyon, all elevations of instruments reported in this study are height above the Strand (14.5 m above sea level). Other papers presenting data from this site (e.g., Kotthaus and Grimmond, 2014b; Ward et al., 2015) reported elevations relative to the mean street height above sea level for the measurement footprint (10.6 m above sea level). In this paper, the former are used within the calculation of CO_2 storage and the latter are used in stability and vertical CO_2 flux.

As CO_2 storage and vertical flux involve processes at the micro to local-scale, the air sampling heights ($6.5 \leq z_i \leq 46.4$ m a.g.l) were chosen to span from within the urban canyon to the top of the eddy covariance tower (z_h, height A, Fig. 1d); in other words, within the roughness sublayer and inertial sublayer. According to a commonly used rule of thumb, the base of the inertial sublayer is 2–3 times the mean roughness element height (Roth, 2000; Grimmond et al., 2004). With a mean element height, z_b, within 500 m of KSSW and KSNW of 21.7 m and 21.8 m respectively (Lindberg and Grimmond, 2011), the sampling heights span $z_i/z_b = 0.30–2.14$.

The 8-point vertical profile system (Fig. 1d) was installed at KSSW and KSNW to allow air to be sampled at a total of 16 locations (ten for a vertical profile, five for two horizontal profiles, one of which was designated an inter-comparison point (IC, Fig. 1c) with one air intake from each valve array). CO_2 concentration is measured at each location at 2 Hz for 75 s by an infrared LI840 gas analyser (LI-COR Biosciences, USA), with each 8-point profile completing a cycle in 10 min (for further instrumentation details see Supplementary material S.4). The first 10 s of data for each run were removed to prevent contamination by the previous sample and the remaining concentrations averaged to give a '1 min value'. Data reported here were not gap filled. Reasons for data gaps include physical component failure (e.g., burnt out air pumps), theft or failure of on-site computer, electricity supply failure, extensive building works, instrument removed for calibration and software problems. Other measurements used in this paper include shortwave radiation measured at KSSW and KSNW by net radiometers (CNR4 and CNR1 respectively, Campbell Scientific, USA), wind speed and direction measured at KSSW by a 2D sonic anemometer (WXT520, Vaisala, Finland) and by 3D sonic anemometers (KSSW and KSNW: CSAT3, Campbell Scientific, USA; KSB: R3-50, Gill, UK). Calculated quantities used to classify CO_2 storage values include z'/L, a measure of atmospheric stability, where z' is the height of the CSAT3 above ground less the zero plane displacement height, and L is the Obukhov length. The ratio z'/L was calculated at 30 min resolution using data from KSSW CSAT3 (Kotthaus and Grimmond, 2014a).

2.3. Climate

The conditions under which this study was undertaken include: prevailing winds from the southwest (for 2012 to 2014, mean wind speed 3.98 m s^{-1}, WXT520, KSSW, height A, Fig. 1d); and an air temperatures range of −2.1 to 31.3 °C (mean annual air temperatures of 11.2 and 12.7 °C in 2013 and 2014 respectively). For more details see Supplementary material S.5.

The observed atmospheric stability (see Section 2.2) was classified as: extremely unstable: $-1 < z'/L \leq -0.1$, unstable: $-0.1 < z'/L \leq -0.05$, unstable/near neutral: $-0.05 < z'/L \leq -0.01$, neutral: $-0.01 < z'/L \leq 0.01$, or stable: $0.01 < z'/L \leq 1000$. Kotthaus and Grimmond (2014a) showed that stable atmospheric stratification is rare for this central urban area. The infrequent stable conditions (3.2% of all periods June 2012 to Dec 2014) occurred predominantly at night (20:00 to 06:00 GMT) in autumn and winter, when vertical fluxes are low (Ward et al., 2015) and the relative importance of the storage term is accordingly expected to be enhanced. Although, nocturnal release of storage heat from the urban fabric (Grimmond and Oke, 1999) is usually sufficient to maintain fully turbulent conditions overnight, observations at this site found periods of stability throughout the year and at all hours of the day. For more details of the stability characteristics of the site, see Supplementary material S.5.

3. Diurnal, hebdomadal and seasonal cycles in CO_2 storage

The forcings affecting ΔC_{SS} and ΔC_{SP} vary at daily, weekly and seasonal timescales. The general properties of ΔC_{SP} are illustrated for a typical weekday and rest day (e.g., weekend, holiday) in June, 2013 (Fig. 2). These were dry, sunny days, with minimal CO_2 emissions above roof height as there was low building occupancy (university summer vacation) and no need for building heating.

3.1. Example days

The 10 min ΔC_{SP} data for 2013/153 to 154 tended (80% of values) to vary between −0.52 and 0.56 μmol m^{-2} s^{-1} (Fig. 2a) within an overall range of ±1.6 μmol m^{-2} s^{-1}. Despite the difference in environment, this is comparable to data reported by Iwata et al. (2005), who calculated mean daily storage of 0.32 μmol m^{-2} s^{-1}, with skew of −0.32, using a 30 min profile of 6 heights in the Brazilian rainforest. Larger values (−20 to 5 μmol m^{-2} s^{-1}) were observed by Araujo et al. (2010), who made 5 s resolution measurements at 6 heights, cycling through the profile in 15 min. They noted a difference in the diurnal cycle of storage depending on whether the profile was situated on a plateau, slope, or valley bottom, with the latter having the most clearly defined cycle of accumulation overnight and dispersal during daylight hours. Similar cycles have been reported from a number of forested sites in Europe (Aubinet et al., 2005), albeit with a smaller range (−5 to 3 μmol m^{-2} s^{-1}). Unlike the aforementioned rural studies, no clear diurnal or hebdomadal cycle in the instantaneous ΔC_{SP} values was observed for these particular days (Fig. 2a) at the Strand. Calculated CO_2 storage values were exceedingly noisy, with increases in ΔC_S tending to be followed by decreases. There are some small visual and skew differences in the frequency-size distibutions (Fig. 2b) between weekend (dashed blue line) and weekday (solid red line)

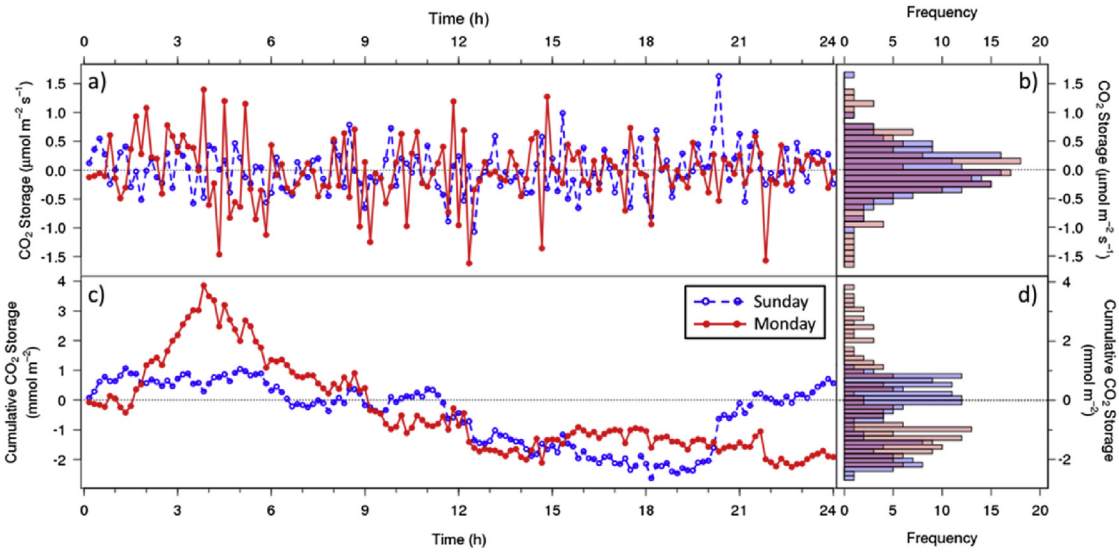

Fig. 2. Characteristics of weekday (red, solid line) and weekend (blue, dashed line) CO_2 storage at the King's College London site (KS), London, UK, for two example days in June 2013 (key, upper right (c)). (a) CO_2 storage from 10 min cycle $[CO_2]$ profile data (all heights, Fig. 1d) and (c) the running sum for two different days: 2013/153 (dashed blue line, Sunday) and 2013/154 (solid red line, Monday). (b) & (d): histograms (number of counts per bin, red: weekday, blue: weekend) of (a) (bin width 0.1 μmol m^{-2} s^{-1}) and (c) (bin width = 0.15 mmol m^{-2} s^{-1}). (For interpretation of the references to colour in this figure legend, the reader is referred to the web version of this article.).

values (skew of 0.42 and −0.24 for Sunday 2013/153 and Monday 2013/154 respectively).

Changes in frequency (Fig. 2d) impact the cumulative CO_2 storage (Fig. 2c). Weekend ΔC_{SP} accumulated nocturnally is lost during the afternoon. The weekend cycle is more muted than the weekday one. The latter has a larger peak but shorter nocturnal accumulation. From mid-rush "hour" there is loss. The differences between the weekday and weekend ΔC_{SP} may relate to traffic volumes or traffic timing. However, comparison of the change in $[CO_2]$ with time at each profile height, z_i, and traffic volume (Automated traffic count, ATC, 250 m to the north east of KSSW) for 2012/151–2013/150 found no relation using a linear model fitted by least-squares between the two at any profile height ($R^2 < 0.01$, where R^2 is calculated as the residual sum of squares divided by the total sum of the squares and subtracted from one). The absolute value of the change in $[CO_2]$ with time appeared to increase with increasing traffic volume, with the strongest relation found at the lowest measurement heights. However, no R^2 for a linear regression of the change in $[CO_2]$ with time on traffic volume exceeded 0.05.

3.2. Seasonality

This section compares ΔC_S calculated via the two approaches described in Section 1.1 as they are commonly implemented; in other words, ΔC_{SS} from $[CO_2]$ measurements made by a fast response infra red gas analyser at one point high above the height of the local roughness elements (e.g., Nemitz et al., 2002; Crawford and Christen, 2014), and ΔC_{SP} from $[CO_2]$ measurements made by a closed path infra red gas analyser, with air samples drawn from multiple locations in a vertical profile (e.g., Aubinet et al., 2005).

The diurnal cycle (columns, Fig. 3) of ΔC_S is not constant throughout the year (rows, Fig. 3) and varies with measurement method (Fig. 3a/b vs. c/d). The ΔC_{SP} values calculated from 2 Hz LI840 data averaged to 1 min values between 2012/160 and 2013/155 were averaged by hour of day and month of year. The majority (80%) of these hourly/monthly medians were within ±0.13 μmol m^{-2} s^{-1} (Fig. 3); minor in comparison to median turbulent vertical CO_2 flux for the Strand of ~35 μmol m^{-2} s^{-1} (Kotthaus and Grimmond, 2012). For median ΔC_{SS} values calculated in the same fashion from 10 Hz LI7500 data over the same period, 80% of values were within 0.01–0.11 mmol m^{-2} s^{-1}, three orders of magnitude larger and significantly less equally distributed about 0. The difference between ΔC_{SP} (LI840) and ΔC_{SS} (LI7500) is also present for the hourly mean values, with 80% of ΔC_{SP} values within ±0.16 μmol m^{-2} s^{-1} when calculated from LI840 data, and between −0.19 and 0.00 mmol m^{-2} s^{-1} for ΔC_{SS} LI7500 data for the same period. Not only does the ΔC_{SS} calculated from the LI7500 data have a greater range of values, it also has a greater (negative) skew than ΔC_{SP} calculated from the LI840 data. The impact of sampling interval and sensor response time are explored further in Section 6.

3.2.1. LI840 ΔC_{SP}

Both hourly/monthly mean and median ΔC_{SP} calculated from LI840 data show a clear diurnal cycle, the magnitude and timing of which is seasonally variant (rows, Fig. 3a, b). Peak ΔC_{SP} is observed in the morning, followed by a midday trough and less clearly defined evening peak. Overnight storage values tend to be negative during the colder months (October to April) and weakly positive otherwise (May to September). The timing of the morning peak is closest to midday during January (~08:00 GMT) and furthest in June (~03:00 GMT), with a steady transition between the two that suggests that the dominant forcing is boundary layer stability and mixing, rather than anthropogenic behaviour. Comparison of hourly median CO_2 storage for weekdays and weekends for June–August 2012 found no difference in the timing of the peak or trough CO_2 storage values despite higher overnight and lower daytime traffic volume on weekends.

Negative overnight values during winter indicate loss of CO_2 from the canyon airspace and coincide with minima in the observed diurnal cycle of F_{CO2} (Kotthaus and Grimmond, 2012, Fig. 14a). This is unlikely to be due to photosynthetic uptake. An alternative explanation is drainage flow away from the canyon below z_h, potentially towards the River Thames; however, the EC measurements are predominantly unstable at KSSW even during overnight winter periods (Supplementary material S.5). Within canyon temperatures in winter (2012/335 to 2013/059) exceeded

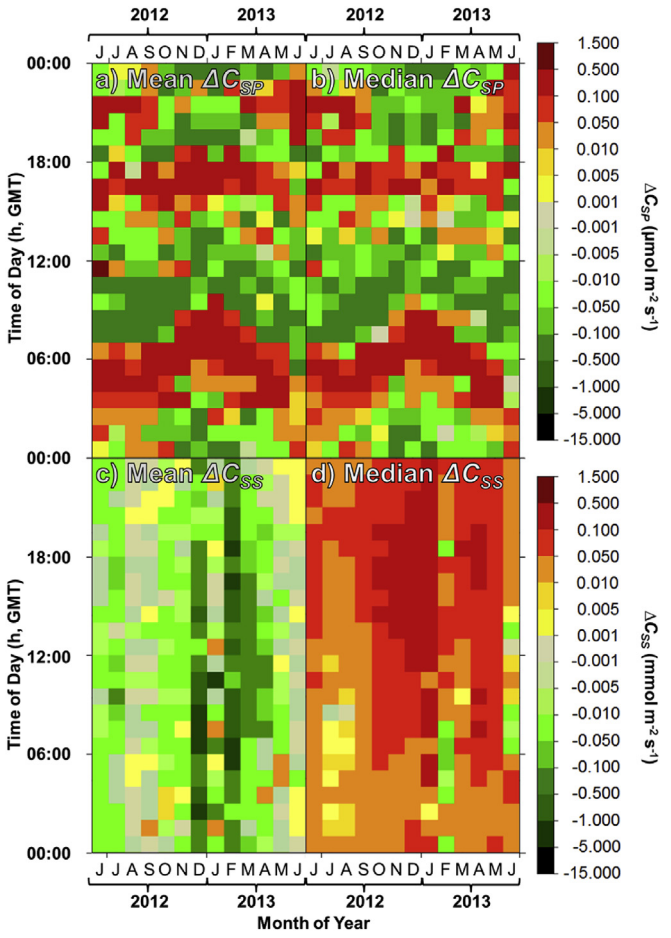

Fig. 3. Diurnal (y-axis) and seasonal (x-axis) cycle of CO_2 storage (key: far right) at KS, London, UK. (a) hourly/monthly mean CO_2 storage calculated from profile measurements (ΔC_{SP}), (b) hourly/monthly median ΔC_{SP}, (c) hourly/monthly mean CO_2 storage calculated from measurements at a single height (ΔC_{SS}), (d) hourly/monthly median ΔC_{SS}. ΔC_{SP} calculated from $[CO_2]$ measured at all heights (Fig. 1d) with a cycle time of 10 min ΔC_{SS} calculated from $[CO_2]$ measured at height A (Fig. 1d) by LI7500 at 10 Hz. All data measured 2012/159 to 2013/154 and aggregated by month of year (x-axis) and hour of day (y-axis). The ΔC_{SP} data are in units of μmol m^{-2} s^{-1} and the ΔC_{SS} data in mmol m^{-2} s^{-1}.

those measured at z_h by ~0.8 °C at all times of day on both weekdays and weekends and it is suggested that the losses are either due to sustained thermally induced turbulence as described by Velasco and Roth (2010), or the release of intermittent thermally induced 'bursts' of high CO_2 air from the canyon (Supplementary material S.6) as described by Salmond et al. (2005) and Lietzke and Vogt (2013). The temporal resolution of the ΔC_{SP} measurements is not sufficient to distinguish the two and the question is revisited in the following section.

3.2.2. LI7500 ΔC_{SS}

The ΔC_{SS} calculated from LI7500 data shows a much weaker diurnal cycle relative to seasonality and a much greater difference between mean and median hourly values (rows Fig. 3c, d). Hourly means tended to be negative whilst hourly medians tended to be positive, with the difference between the two greatest for November to January. In other words, data during this period had a greater range of values and was more negatively skewed. The larger positive values could be due to greater emissions from space heating, whereas the intermittent but strongly negative values lend credence to the hypothesis of CO_2 venting from the street canyon.

Previous work (Lietzke and Vogt, 2013) indicates that even for street canyons with height:width ratios as low as 0.34–0.70, strong wind shear across the top of a canyon can act as a 'lid', preventing turbulent mixing out of street level emissions. Intermittent air parcels break through this lid (Caton et al., 2003) and vent high CO_2 air from the canyon into the airspace above. Periods with high shear (and high friction velocity) might therefore be expected to show negatively skewed CO_2 storage within the canyon relative to periods with lower shear. The friction velocity calculated from data measured at KSSW was used to classify the change in $[CO_2]$ with time at three locations within and above the Strand canyon (Fig. 4). The change in CO_2 concentration with time ($\Delta[CO_2]/\Delta t$) was chosen in preference to CO_2 storage as the absolute value of the latter depends upon the vertical separation of the measurement points. Data collected at point J (Fig. 1d), the lowest measurement location, showed the least change in either magnitude or variance of $\Delta[CO_2]/\Delta t$ with increasing friction velocity (Fig. 4, Fig. S.7 in Supplementary material S.7). $\Delta[CO_2]/\Delta t$ measured above the canyon and at canyon half-height (A and G respectively, Fig. 1d) decreased from approximately 1.5 to 0.0 μmol m^{-3} s^{-1} with increased friction velocity (0.1–0.5 m s^{-1}, S.7), however there was no consistent shift in skew or sign. Results indicate that increased friction velocity affects the mixing down to about half the canyon height whereas the lowest levels are effectively sheltered.

4. Built form and wind direction

CO_2 storage depends not only on emissions but also on the efficacy of transport processes. In Section 3.2.2 the lower measurement levels were shown to be effectively sheltered from shear-based turbulence, even at high above-canyon wind speeds. In this section the effect of above-canyon wind speed and direction on within-canyon CO_2 storage and CO_2 transport is examined in more detail.

The asymmetric Strand canyon runs east-northeast to west-southwest (Fig. 5a), bifurcated opposite the western half of the Strand building by a church (St Mary le Strand). Airflow through the canyon within 20 m of the ground may, depending on the time of year, be deflected or attenuated by the trees lining the street and, depending on the time of day, be blocked or shifted by the large number of buses on the southern half of the roadway (i.e., the side of the measurements). Both sides of the street vary in height and the canyon is not of uniform width; due to the presence of the

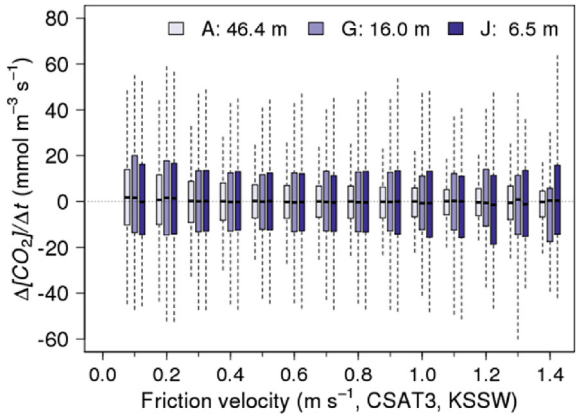

Fig. 4. Change in CO_2 concentration with time ($\Delta[CO_2]/\Delta t$) by above-canyon friction velocity for three different heights (A, G and J, see Fig. 1d) within the Strand canyon (London, UK, mean building height, $z_h = 21$ m) calculated from 10 min $[CO_2]$ profiles collected 2012/159 to 2013/154. Bar: median; box: interquartile range; whiskers: 5th to 95th percentile.

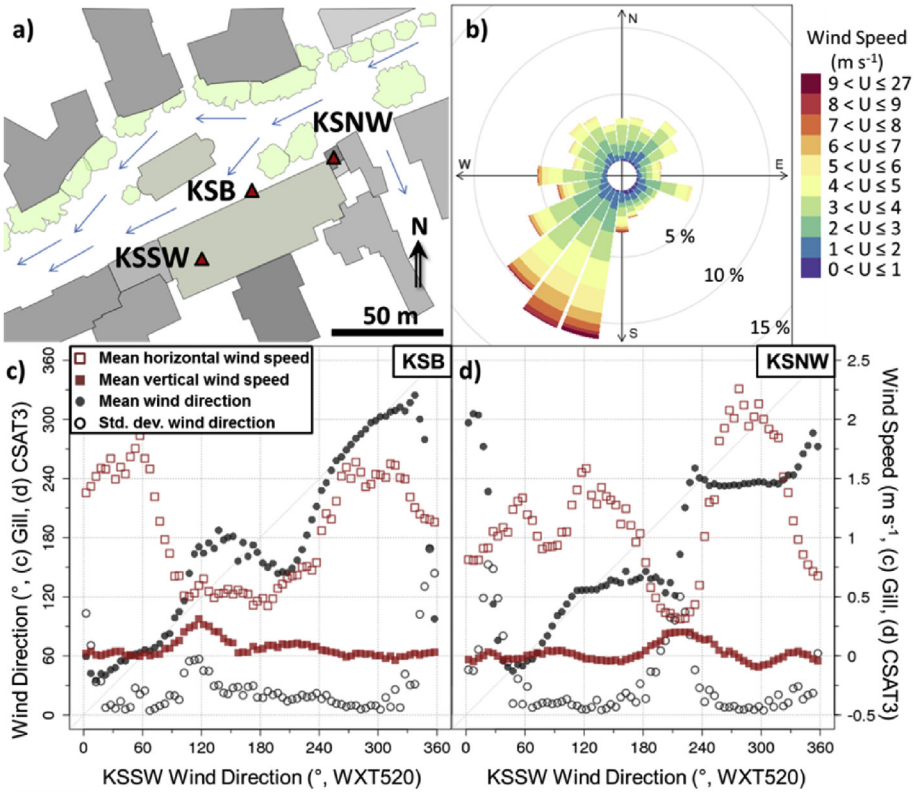

Fig. 5. Wind speed and direction data relative to the built form of the Strand, London, UK. (a) Plan view of the Strand canyon buildings (grey), trees (green) and traffic flow (blue arrows) with locations of wind monitoring sites (red triangles) KSSW, KSB, and KSNW (Fig. 1c); (b) Horizontal wind speed (U, m s^{-1}) and direction measured at KSSW (CSAT3, 2013/100 to 2014/100); (c, d) 30 min wind direction (circles, mean: filled; standard deviation: open) and speed (squares, vertical: filled; horizontal: open) binned by wind direction (°, KSSW, WXT, 46.4 m above Strand level) 2013/100–2014/100, for (c) KSB (Gill, 19.0 m) and (d) KSNW (CSAT3, 20.5 m). (For interpretation of the references to colour in this figure legend, the reader is referred to the web version of this article.).

church and the curvature of the road it varies from 13 to 46 m. Comparisons between wind direction and CO_2 storage in this section are therefore limited to this case study and are unlikely to be widely applicable.

As wind speed and direction measurements at KSB (Fig. 5a) were not available throughout 2012/159–2013/154 (the focus of the previous section) a comparison (2013/100 to 2014/100) of data collected by the WXT520s at KSSW and KSNW for both time periods was undertaken. This found that neither the overall wind direction distribution nor the within canyon response differ significantly from year to year.

Wind speed and direction measurements taken at KSSW and KSB are assumed to be representative of the local and canyon air flow respectively, whilst measurements at KSNW represent either the intersection to the east or the canyon to the west. The prevailing wind was from the south-southwest (~210°), approximately 30° off parallel to the canyon (~245°, Fig. 5b). Although this direction had the highest mean above canyon wind speed, horizontal wind speeds measured at KSNW were at their lowest due to sheltering by the Strand building (Fig. 5d) and were scattered rather than channelled. Horizontal wind speed minima (KSB: 150°, KSNW: 240°) are measured at each site when in the lee of the Strand building and are associated with increasing $[CO_2]$ with time ($\Delta[CO_2]/\Delta t$) for heights G-J (Fig. 6).

Channelling of airflow does not occur for wind from the north east quadrant at either KSB or KSNW, potentially due to the more open canyon structure around the eastern intersection (Fig. 5a). This sector is associated with a horizontal wind speed minimum and a peak in vertical wind speed. The most negative (downward) vertical wind speeds were measured when above canyon wind at 290° was channelled to 240° (Fig. 5d), perhaps indicating the presence of a spiral vortex. Both the minimum (290°, KSNW) and the maxima (120°, KSB; 210°, KSNW) in vertical wind speed are associated with a reduction in $\Delta[CO_2]/\Delta t$ at all $z_i \leq 16$ m (heights G to J, Fig. 1d), suggesting that rather than just recirculating and trapping emissions, vortices act to reduce CO_2 with time at both windward and leeward walls. For discussion of the change in variability of $\Delta[CO_2]/\Delta t$ with height and above-canyon wind direction, see Supplementary material S.8.

5. Sample locations

One of the first decisions when preparing to make $[CO_2]$ profile measurements is the number and position of sample locations. We discuss in this section how these decisions were made. The aim, in general, is to accurately characterise the shape of the vertical $[CO_2]$ profile with as few sampling points as possible to minimise data loss due to switching, and installation and running costs. Ideally measurements would be more densely spaced where the concentration changes rapidly with height, and more sparse where $[CO_2]$ is more constant with height. It is commonly accepted that for rural profiles, measurement density should be greater closer to the ground as the major source of CO_2 is sub-surface respiration and the atmospheric profile of the gas changes more quickly at lower elevations (Wofsy et al., 1993; Goulden et al., 1996; Jarvis et al., 1997; Mölder et al., 2000; Iwata et al., 2005; Vogt et al., 2006; Araujo et al., 2010). Six-hourly, median vertical $[CO_2]$ profiles measured at the Strand during June and November/December 2012

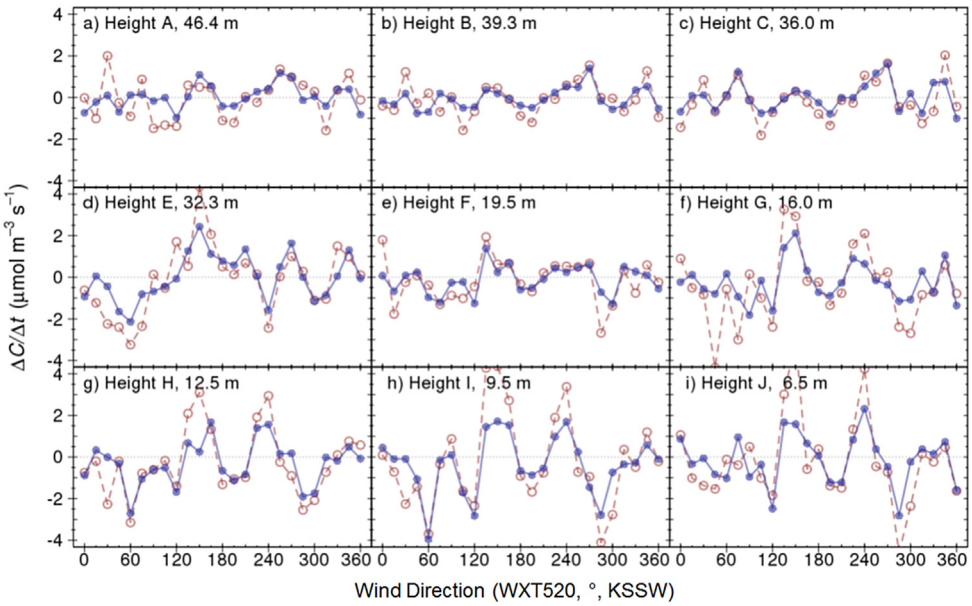

Fig. 6. Median and mean change in CO_2 concentration with time ($\Delta[CO_2]/\Delta t$, y-axis, μmol m^{-2} s^{-1}) within and above the Strand canyon (London, UK) (see Fig. 1d) sorted by above-canyon wind direction (x-axis, °, WXT520, KSSW). Each plot contains $\Delta[CO_2]/\Delta t$ calculated from data at a different location (upper left) in the vertical $[CO_2]$ profile during the period 2012/159–2013/150.

(Fig. 7a) suggests this may not be the case for high-density urban environments. The difference between median $[CO_2]$ observed at the top of the tower (z_i = 46.4 m above Strand level) and the concentrations measured along the profile, with measurement height relative to the mean building height (z_b), shows weekday concentrations in the canyon relative to those measured at z_i = 46.4 m tend to be higher. This can be explained by the greater volume of traffic emissions as the difference is most pronounced in the daytime periods (06:00–12:00 GMT and 12:00–18:00 GMT) during weekdays – the time when traffic volumes are largest. The morning period reveals clearly enhanced concentrations during the summer period compared to the winter period in the lowest layers ($z_i/z_b < 1$) for both weekends and weekdays, while in the afternoon, this seasonal shift is only evident for the weekdays. In winter within-canyon $[CO_2]$ for the weekend 12:00–18:00 GMT period exceed those of the weekday, however the difference is within the standard deviation of the data (Fig. 7b).

In Fig. 7a, rather than the smooth, exponentially decreasing concentration curve with height observed in Basel (10 locations spanning 0.17 to 2.3 times the mean building height z_b, Lietzke and Vogt, 2013), median $[CO_2]$ shows a sharp transition at the Strand building roof level (Fig. 7a and 30.5 m, dot-dash horizontal red line), and potentially another close to the mean building height (Fig. 7a and 21 m, dotted horizontal blue line) during the day (06:00–18:00 GMT). The difference between observed profiles in Basel and London is likely to be due to the greater street canyon depth at KS; the height:width ratios for the street canyons in Basel and London are 0.34–0.70 and 0.74–1.28, respectively. Lietzke and Vogt (2013) characterised the flow regime in Basel as 'wake interference' (Oke, 1987), leading to greater mixing out of canyon emissions compared to the 'skimming flow' conditions likely to dominate at KS. The latter would result in a fast moving 'lid' of air over the roof of the Strand building during the prevailing south-westerly winds and an active vortex within the canyon, leading to two fairly internally homogenous flow regimes, with some exchange at the interface at roof height. This is observed to some extent in Fig. 7a; however, the difference between above and within canyon $[CO_2]$ is more apparent in the standard deviation of the measured $[CO_2]$ for each time period and height (Fig. 7b). Measurements at or below the Strand building height have consistently higher variance than those above for both summer and winter, weekdays and weekends. This suggests that the $[CO_2]$ profile in an urban street canyon with near 1:1 height:width ratio could be adequately measured by two or three points, provided they were placed appropriately.

This 'small sample' hypothesis is tested by extending the analysis of Yang et al. (2007) to the urban $[CO_2]$ profile. The method consists of defining a CO_2 storage time series calculated from a particular configuration of sample inlets as 'best practice' (ΔC_{SBP}) and assessing other configurations based on how closely the calculated ΔC_S from each configuration agree with ΔC_{SBP}. In this study, ΔC_{SBP} was defined as the CO_2 storage calculated using data from all ten vertical profile locations. All configurations included z_h, co-located with the eddy covariance system, as such a tower-top measurement is commonly present at micrometeorological sites observing turbulent fluxes. Configurations were grouped by number of sample locations included in the CO_2 storage calculation, (e.g., all configurations with three sample locations fall in 'Group 3'). Storage was calculated as the change in $[CO_2]$ weighted by the vertical span for each height and divided by the cycle length. The vertical span (Δz_i) for a sample location z_i was defined as $(z_{i+1} - z_i)/2 + (z_i - z_{i-1})/2$, except for the lowest height, where the span extended to ground level, and the uppermost height, where the span stopped at $z_i = z_h$ = 46.4 m.

CO_2 storage was found to be highly variable with configuration. The ΔC_S time series for each configuration were compared with ΔC_{SBP}. The configurations within each group with the lowest (Fig. 8a) and highest (Fig. 8b) root mean squared error (RMSE) were considered as the 'best' and 'worst' configurations respectively. Configurations were found to perform best if the inlet heights were evenly distributed and the vertical span for each available sample point was maximised. In other words if few inlet points are present, the configurations with the greatest distance between the inlets showed the best performance (Fig. 8a). This is in contrast to previous rural work (e.g., Iwata et al., 2005) which has tended to cluster sample points at the base of the profile. Configurations with

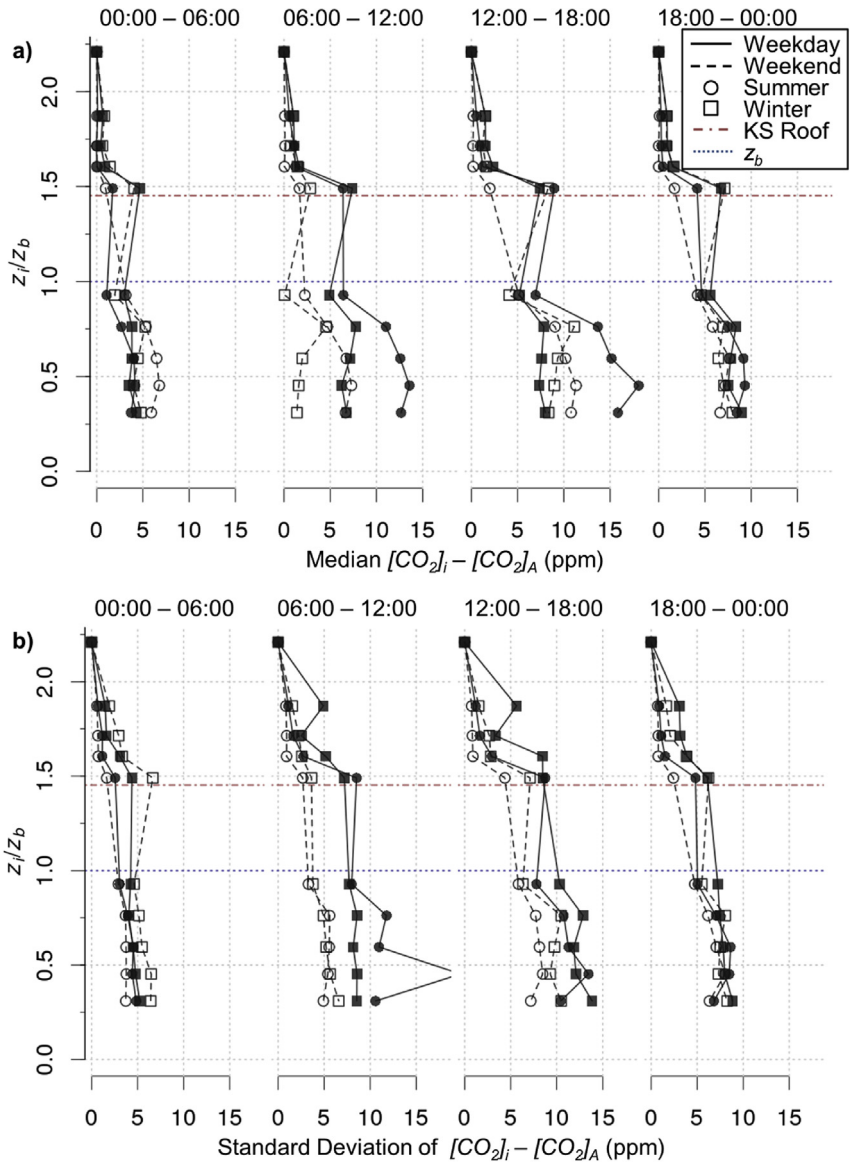

Fig. 7. (a) Strand (London, UK) median enhancement of CO_2 concentrations ($[CO_2]$) in ppm (x-axis) at each height z_i (heights A to J, Fig. 1d), $[CO_2]_i$, relative to $[CO_2]_A$ measured at z_h, (height A, Fig. 1d) binned by time of day (left to right, with all times in GMT: 00:00–06:00, 06:00–12:00, 12:00–18:00, 18:00–00:00) with (y-axis) the height of inlet (z_i) relative to mean building height (z_b, dotted horizontal blue line). Solid symbols/lines: weekday; hollow symbols/dashed lines: weekend. Circles: summer (2012/156 to 183); squares: winter (2012/324 to 351). Horizontal dot-dash red line: Strand building height. (b) As (a), but standard deviation. (For interpretation of the references to colour in this figure legend, the reader is referred to the web version of this article.).

'bad performance' (highest RMSE, Fig. 8b) have sample points clustered towards the top of the profile, adding little new information with each new location.

The 'value' of each additional sample point can be assessed by comparing the coefficients of the regression of the ΔC_S calculated from each group's best configuration onto ΔC_{SBP} (Fig. 9). Increasing the number of sample points from 1 to 2 increases the coefficient of determination (R^2) from 0.15 to 0.80 provided that the second sample point is placed appropriately. In this study this was found to be at just over half the height of the street canyon (height F: 19.5 m; canyon wall height: 34.5 m = Strand building height of 30.5 m + safety wall height of 4.0 m). This supports the 'small sample' hypothesis, namely that for street canyons with height:-width ratios of approximately 1:1, the urban environment can be adequately measured, and perhaps, modelled, as a two-layer system of above and within-canyon air masses with a transition zone at roof level. It is not necessary to monitor the concentration all the way down to street level as the air within the canyon is well mixed and responds quickly to ground-level changes in $[CO_2]$. As expected, air above roof level is less responsive to street canyon processes and measurements made at 2–3 times mean building height should not be considered directly representative of processes within the street canyon below. The assumption required for the single height calculation of CO_2 storage, also known as the storage flux correction, is not valid – at least one other measurement point is required.

6. Sensor response and sampling interval

In this section, the measurement time resolution necessary to capture the majority of the CO_2 signal is assessed using the wavelet power spectrum. The effect of under sampling or inadequate sensor

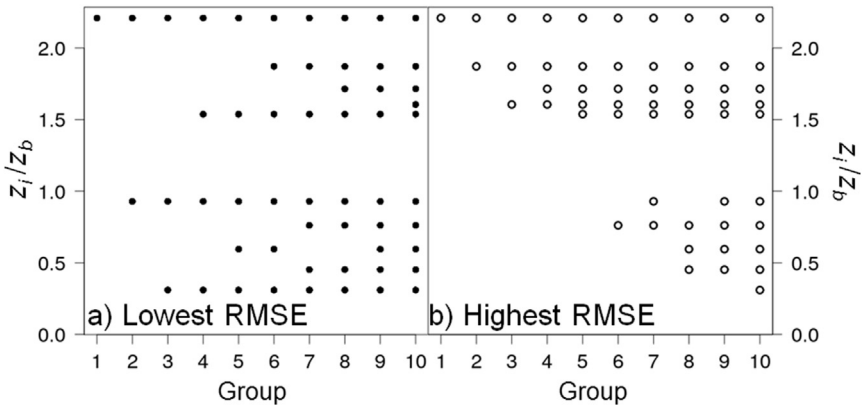

Fig. 8. The height of inlet (z_i) relative to mean building height (z_b) as a function of configurations for each group with (a) lowest and (b) highest root mean squared error (RMSE) when the resultant CO_2 storage time series is regressed onto the benchmark CO_2 storage time series (2012/150–2013/153, heights A-J, KS, London, UK, see Fig. 1) calculated from data averaged to 30 min. Group number indicates number of inlets for a configuration.

response time is simulated by subsampling and progressively smoothing a *[CO_2]* time series. The loss of calculated CO_2 storage with decreasing time resolution is predictable and is shown to be correctable to an extent.

Continuous, high frequency (10 Hz) *[CO_2]* measurements were made by LI7500 at heights A and F (Fig. 1d) from 2013/073 onwards. Days 2013/347–2013/365 were chosen for analysis as the campus was closed and rooftop emissions were likely to be minimal. Winter days were chosen despite the sensitivity of the open path sensor to inclement weather due to the greater probability of stable periods (Fig. S.2 in Supplementary material S.5) during which CO_2 storage is expected to be significant relative to the vertical flux.

Data were divided into 30 min periods for wavelet analysis. Wavelet analysis has a number of advantages for atmospheric data relative to traditional Fourier analysis when constructing power spectra. Fourier analysis requires regular, complete data sets as any errors or missing values are delocalised throughout the entire spectrum (Farge, 1992). Fourier analysis also has difficulty resolving sudden transitions or aperiodic signals (Farge, 1992), both of which can occur frequently in an urban CO_2 storage time series due to the prevalence of intermittent, strong CO_2 sources. In contrast, wavelet analysis does not delocalise errors, can resolve sudden step changes or spikes (Salmond et al., 2005), and was found to be considerably quicker to compute than the gap-tolerant (Press and Rybicki, 1988) Lomb-Scargle Periodogram.

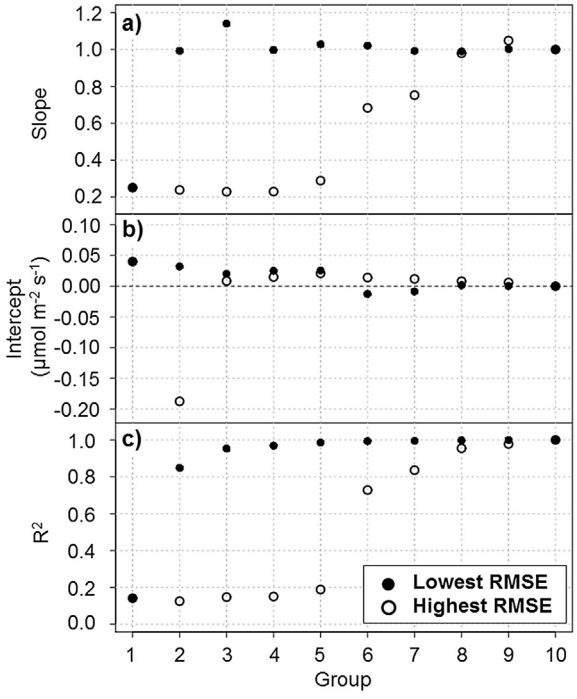

Fig. 9. The (a) Slope, (b) Intercept and (c) coefficient of determination (R^2) for the configurations (Fig. 8) with highest and lowest root mean squared error (RMSE, see key) when regressed onto the (benchmark) CO_2 storage time series calculated from all ten inlets (see Fig. 1d) for 2012/150–2013/153.

Wavelet analysis was conducted on the 10 Hz time series data following Torrance and Compo (1998), and used in-house software, written in R. If a data set of 30 min had fewer than 10 min of continuous data, the data set was rejected for analysis. Data were normalised by subtracting the mean and dividing by the standard deviation of the data set prior to processing. The Mexican Hat wavelet (negative of the second derivative of a Gaussian, appropriately normalized) was applied at 53 temporal scales ranging from 0.2 s to 27.3 min. The Mexican Hat wavelet was chosen as it has previously been used to successfully identify coherent structures in atmospheric turbulence over an urban area (Feigenwinter and Vogt, 2005). Wavelet powers were calculated as the square of the absolute value of the wavelet coefficients, then summed over time and weighted by the original series' variance and number of data points to give the global wavelet spectrum. Global wavelet spectra were binned by frequency and atmospheric stability for each half hourly period (z'/L, height A, KSSW, Section 2.2).

The wavelet power spectra for both ΔC_{SP} and ΔC_{SS} were found to increase as a power-law with frequency (i.e., a linear relationship on a log–log axis), with approximately a 1:1 relation between 0.005 and 0.1 Hz (200–10 s) and approximately 1:2 relation between 0.1 and 0.5 Hz (10–2 s) (Fig. 10a,b). When normalised by the natural frequency the peak spectral energy was found to be between 0.001 and 0.004 Hz (1000 and 500 s or 8–16 min), although this range has higher frequency during neutral and stable conditions for ΔC_{SP} (Fig. 10c, d). There was also a secondary peak at approximately 0.1 Hz or 10 s, above which spectral power declines as an inverse-power law with exponent of approximately −2/3 for all stability classes. It is therefore expected that measurements with a time resolution of better than 1 s should not produce significant improvement in measured CO_2 storage. This was tested by altering the two main controls on the temporal resolution of measured *[CO_2]*: the sensor response time and the logging rate. A correction factor for cases where the required time resolution could not be

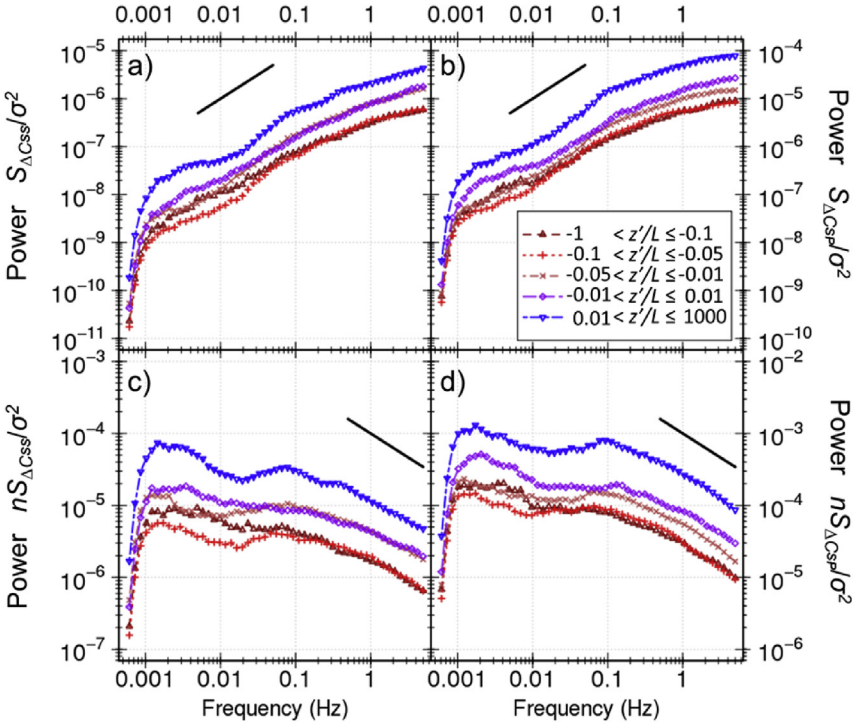

Fig. 10. Global wavelet power spectra S normalised by the variance σ^2 versus frequency in Hz by stability class (key) for (a) CO_2 storage at a single location, ΔC_{SS}, (b) CO_2 storage from a profile, ΔC_{SP}; (c) and (d) as (a) and (b) but normalised by natural frequency (number of cycles, n, in 30 min). For each subfigure a solid black line indicates a power-law exponent: (a & b): 1.00, (c & d): −0.667. Note each y-axis has a different scale. The ΔC_{SS} calculated from 10 Hz LI7500 data at height A (Fig. 1d), ΔC_{SP} from 10 Hz LI7500 data at heights A and F (Fig. 1d), 2013/347–2013/365. Stability classes correspond to z'/L (effective height z' over the Obukhov length L) ranges as follows: extremely unstable: $-1 < z'/L \leq -0.1$, unstable: $-0.1 < z'/L \leq -0.05$, unstable/near neutral: $-0.05 < z'/L \leq -0.01$, neutral: $-0.01 < z'/L \leq 0.01$, stable: $0.01 < z'/L \leq 1000$.

attained is proposed.

The basis of both the sensor response time and sensor logging rate analyses is data from two LI7500 installed at KSSW and KSNW during an intensive observation period between 2014/013 and 2014/043. During this time the sample rate was increased from 10 Hz to 20 Hz to ensure that the normal operating frequency (10 Hz) was resolvable. Different logging rates were simulated by sub-sampling this time series at intervals ranging from 10 Hz to 10 min. To check that the response was not sensor specific, co-located continuous LI840 data (2 Hz) time series were also sub-sampled at intervals up to 10 min. A similar technique was used by Heinesch et al. (2007) to estimate the uncertainty in CO_2 concentration measurements; however, to enable analysis over a larger time range, data in this study were not resampled multiple times. Both LI7500 and LI840 data sets were also used to investigate the effect of sensor response time. This was simulated by smoothing the concentration time series with a modified, single-sided cosine function.

Due to the volume of data it was too computationally expensive to plot the instantaneous values. Instantaneous ΔC_S values at each time resolution were therefore summed over 30 min periods to give the total storage change within each period. The stability of each 30 min period was calculated as the effective height (z') over the Obukhov length (L) (Section 2.2) from data measured at KSSW. There was some indication that CO_2 storage values were lowest for neutral stability but this was not consistent across all time resolutions.

Slowing the sensor response time has the largest impact on calculated ΔC_S between 0.1 and 5 s (Fig. 11a), corresponding to a resolvable frequency of 5 to 0.1 Hz (as the highest resolvable frequency is half the sample rate). This frequency range corresponds to the aforementioned portion of the natural frequency normalised wavelet power spectrum as a function of frequency, best-fit by a power law relation with exponent −2/3. Improving the response time to below 0.1 s does not seem to affect calculated ΔC_S, suggesting that 0.1 s is sufficient. Below 1 s there is little change with increasing smoothing length.

In contrast, on a log–log plot, there is a linear decrease in median absolute half-hourly ΔCs ($|\overline{\Delta C_S}|$) with increasing sampling interval length, t_s, (Fig. 11b) which can be written as:

$$\log_{10}\left(|\overline{\Delta C_S}|\right) = a\log_{10}(t_s) + b \tag{3}$$

where a and b are empirically derived constants with $a = -1.24$ and $b = 1.69$ for the LI7500 data, and $a = -1.14$ and $b = 1.28$ for the LI840 data (all $R^2 > 0.99$). If a time series y_1 has been under-sampled at time interval t_{s1} by an instrument with constants a_1 and b_1, a time series y_2 with desired time interval t_{s2} and measured by an instrument with constants a_2 and b_2, can be estimated from y_1 using:

$$y_2 = y_1 \frac{10^{b_2} t_{s2}^{a_2}}{10^{b_1} t_{s1}^{a_1}} \tag{4}$$

If the instrument is the same for both time resolutions, the factor of 10^b may be omitted as the instrument specific constant, b_2 and b_1, will be the same in both the nominator and denominator of (4). However, if converting between instruments, then the instrument specific constants for each series must be used. This correction is effective at reducing the underestimation of ΔC_S at a sampling interval of 10 min by five orders of magnitude (Figs. 11b and 12). Though simple to apply it is derived from statistical analysis of data only and does not reflect any atmospheric process.

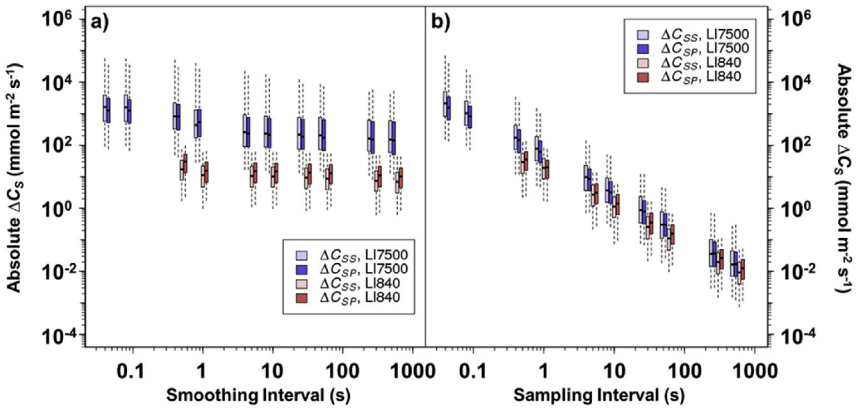

Fig. 11. Absolute value or modulus of half hourly summed CO_2 storage (ΔC_S) calculated with (a) smoothing and (b) subsampling of the CO_2 concentration 31 day (2014/013–2014/043) time series collected by (left to right for each time resolution) LI7500 (20 Hz) and LI840 (2 Hz) continuously at KSSW and KSNW (heights A and F, Fig. 1d). CO_2 storage at a single location (ΔC_{SS}, lighter shading) calculated from data collected from height A only, CO_2 storage from a profile (ΔC_{SP}, darker shading) from both heights. Smoothing and subsampling ranges from none to 600 s. Horizontal bar: median; box: interquartile range; whiskers: 5th to 95th percentile.

7. Interpolation in time and space

Sections 5 and 6 considered the location and temporal resolution of CO_2 concentration measurements necessary to calculate CO_2 storage. In this section, the non-concurrent, spatially irregular CO_2 concentration time series is interpolated onto a regular time/space grid using three different interpolation methods. The interpolated concentration time series and derived CO_2 storage time series are compared to benchmarks and the necessity of interpolating CO_2 concentration time series prior to the CO_2 storage calculation is evaluated.

7.1. Theory

The exact form of the CO_2 storage calculation requires continuous measurements of the $[CO_2]$ profile in time and space (Aubinet et al., 2005). As switched profile measurements are obtained by sampling from several heights sequentially (Mölder et al., 2000), the resulting data are discontinuous at each height. As calculation of the CO_2 storage requires a complete instantaneous profile, further processing can include interpolation of the 'missing' data to provide a continuous concentration time series from which complete profiles can be drawn. Alternatively, the average of the values observed throughout a cycle may be taken as representative of that cycle time period.

Calculation of CO_2 storage also requires integration of the change in $[CO_2]$ over the vertical extent of the profile (Aubinet et al., 2005). This can either be accomplished by weighting the change in concentration at each height by the vertical span over which it is deemed relevant or interpolating to a metre grid and summing over the vertical extent without weighting. The former is mathematically equivalent to taking the average of adjacent heights (e.g., Yang et al., 2007).

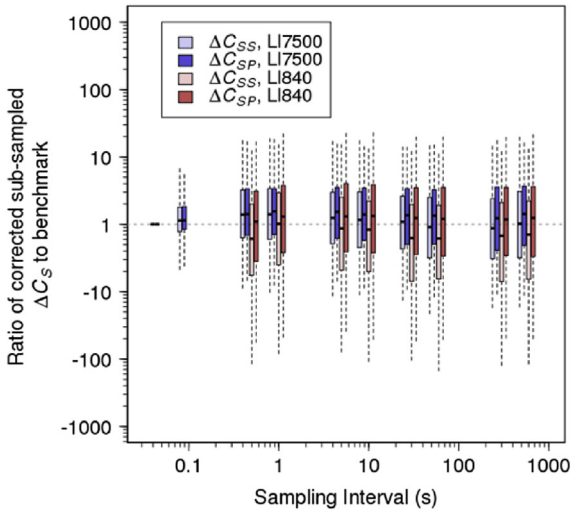

Fig. 12. Ratio of sampling interval corrected (Eq. (4)) absolute 30 min CO_2 storage (ΔC_S) values calculated from subsampled CO_2 concentration ($[CO_2]$) time series to CO_2 storage calculated from 20 Hz non-subsampled data, with subsampling time interval. Original $[CO_2]$ time series from which CO_2 storage values were calculated was collected for 31 days, 2014/013–2014/043, by a two height profile (A and F, Fig. 1d) at 20 Hz (LI7500, continuous, blue) and 2 Hz (LI840, continuous, red). CO_2 storage at a single location (ΔC_{SS}) calculated from data collected from height A only, CO_2 storage from a profile (ΔC_{SP}) from both heights. Bar: median; box: interquartile range; whiskers: 5th to 95th percentile.

7.2. Interpolation in time

The effectiveness of different methods of interpolating $[CO_2]$ in time are evaluated using continuous 2 Hz LI840 $[CO_2]$ measurements (KSSW, z_i = 46.4 m). Data covering half a seasonal cycle (2013/160–365) were split into 75 s 'runs' and processed as described in Section 2.2 to provide a benchmark time series with 8 data points per 10 min. A switched profile time series was simulated by extracting every 8th data point (method illustrated in Fig. 13), which was used as input data for three different interpolation functions.

The first function, termed 'constant' interpolation, assumes all concentrations within 5 min either side of an extracted data point are equal to the extracted value (Fig. 13). This is equivalent to undertaking no interpolation in time but constructing $[CO_2]$ profiles from the measurements closest to a particular time point. The other two functions, 'linear' and 'cubic spline' interpolation were performed using the *approx* and *spline* R functions (R Core Team, 2013) respectively (Fig. 13, 'Linear', 'Cubic'). Leading or trailing missing values were not interpolated.

Interpolated $[CO_2]$ time series regressed on to the benchmark had coefficients of determination $R^2 > 0.98$ (Table 1). The linear interpolation performed the best in terms of R^2 and RMSE, but the constant value method had values for the slope and intercept of the regression that more closely approached 1.0 and 0.0 respectively. The cubic interpolation was the least effective but the difference was small.

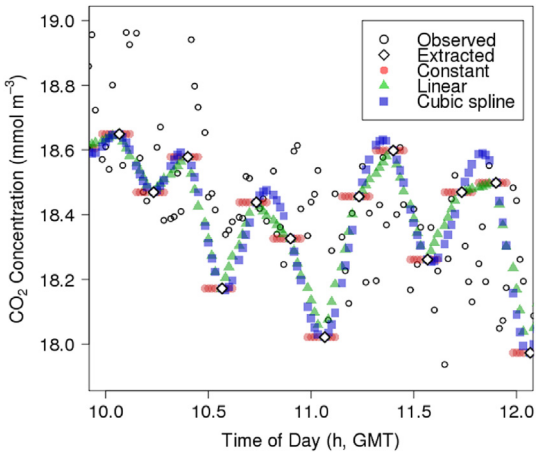

Fig. 13. CO_2 concentration time series observed (key, hollow circles) at KSSW, height A (Fig. 1d); and 'extracted' (key, hollow diamonds) time series consisting of every 8th point of the 'observed' series, and three time series interpolated (Constant, Linear and Cubic spline; see key) from the extracted data for day 2014/038 10:00–12:00 GMT. For details of interpolation see Section 7.2.

The high, positive correlation between interpolated and measured time series for $[CO_2]$ does not hold as well for ΔC_S. None of the R^2 values exceeded 0.05. The ΔC_S calculated from the linearly interpolated time series was closest to the measured values; despite low R^2, the slope and intercept for the regression were 0.95 and 0.00 respectively and it had the lowest RMSE.

The lack of strong agreement between the ΔC_S time series calculated from interpolated data and the benchmark suggests that wherever possible measurements should be made continuously, rather than using a switched profile. Interpolation can adequately reproduce $[CO_2]$; however, as measured CO_2 storage values for a switched profile are typically on the order of 1 μmol m^{-2} s^{-1}, the actual CO_2 storage signal is likely to be smaller than the interpolation error.

7.3. Interpolation in space

Given a 'true profile' with continuous measurements in space and time is unavailable, the full ten height profile was taken as a 'benchmark'. Data from the four heights (A, E, F, J) identified (Section 5) as the 'best' configuration for that number of sample points were divided into 10 min profiles time-centred on the $z_i = 46.4$ m a.g.l. (height A, KSSW) observation and were not interpolated in time. Each 4 height, 10 min vertical profile was interpolated to the remaining six sample points (B, C, D, G, H, I). The interpolation between observations included: linear, cubic and none (i.e., $[CO_2]$ at the interpolated heights were assumed to be the same as $[CO_2]$ at A, E, F or J).

Linear regression was performed between the interpolated and the measured time series for each interpolated height and interpolation method (Table 2). When summed over all interpolated heights for each interpolation method, the lowest RMSE (51.7, 58.3, 58.6 ppm) was when linear interpolation was used, followed by no interpolation and cubic interpolation, respectively (Table 2). The linear interpolation was poorest for the sample points C, D and G ($R^2 = 0.86–0.87$). Both the 'none' and cubic interpolation improve with decreasing height; however, this may be due to the choice of sample points. Due to the larger vertical separation between A and B–D than E and B–D, the latter had a much greater impact upon the 'none' (concentrations taken to be equal to the closest extracted sample point) and cubic interpolations at B–D than the former, despite concentrations measured at B–D often being more similar to A (Section 5) (Table 2). If B–D are considered to be 'closer' to A for the purposes of the 'no' interpolation, the RMSE for the profile drops to below that of the linear interpolation. Whilst the linear interpolation still performs best in the canyon, simple span weighting is more effective above. All methods perform acceptably ($R^2 > 0.8$) for all heights and could be applied without prior knowledge of the profile shape. If the typical profile shape is known and there are obvious physically induced 'break points' in the vertical profile, span weighting to the breakpoints and not to the midpoints between sample locations is the preferred method of spatial interpolation.

Table 1
Coefficient of determination (R^2), Slope, Intercept, Root Mean Squared Error (RMSE) and Degrees of Freedom (DoF) for a linear regression of an interpolation in time of an extracted (Fig. 13) $[CO_2]$ time series on to the benchmark time series (Fig. 13). CO_2 storage time series were calculated from interpolated $[CO_2]$ time series. All values given to 3 s.f.

	Interpolation method	R^2	Slope	Intercept	RMSE	DoF x10^3
CO_2 Concentration (mmol m^{-3})	None	0.987	0.993	0.131	0.151	181
	Linear	0.989	0.992	0.146	0.140	210
	Cubic	0.987	0.992	0.136	0.151	210
CO_2 Storage (mmol m^{-2} s^{-1})	None	0.000	0.000	0.022	7.73	26
	Linear	0.030	0.945	−0.002	5.34	209
	Cubic	0.011	0.601	−0.001	5.39	209

8. Contribution of ΔC_S to Net Ecosystem Exchange (NEE)

The observed vertical flux of CO_2 (F_{CO2}) at KSSW (Fig. 1c) varies both diurnally and seasonally (Kotthaus and Grimmond, 2012; Ward et al., 2015). When aggregated by hour of day and month of year (Fig. 14a), mean F_{CO2} is always positive. Minimum values (<10 μmol m^{-2} s^{-1}) occur between 01:00 and 05:00 GMT in summer (June–August). Though fluxes remain high throughout the day, maximum F_{CO2} values are observed just after midday (12:00–15:00 GMT) during all seasons, with those during the winter (December–February) 60–100 μmol m^{-2} s^{-1} higher than those in summer.

Addition of a storage term calculated from a switched vertical profile to the vertical flux (subset June 2012–May 2013, Fig. 14b) does not appear to alter the diurnal or seasonal pattern of emissions. Appoximately 67% of hourly/monthly flux values were altered by less than 2.5% by the addition of switched ΔC_{SP}. The greatest impact (flux values altered by >5%) was overnight (01:00–05:00 GMT) between July and November, 2012, when vertical fluxes were at their lowest; however, there is no overall inverse relation between size of the vertical flux and percentage contribution by ΔC_{SP}.

Addition of a storage term calculated from measurements made at a single height (A, Fig. 1d) to the vertical flux (subset June 2013–June 2014, s) gives unrealistic estimates of the net emissions, particularly between 03:00–09:00 GMT December 2013 to March 2014 when the incidence of stable conditions was greatest (S.5). The ΔC_{SS} values were found to be 1 to 10 times the magnitude of F_{CO2} and consistently opposite in sign (Figs. 3c and 14a). If accurate, this would suggest that either the urban environment is a substantial CO_2 sink or that the majority of urban CO_2 emissions are transported horizontally below the flux measurement height. Given the low vegetation fraction (Ward et al., 2015) and the lack of a horizontal CO_2 gradient within the canyon of comparable magnitude to the vertical CO_2 gradient (not shown), neither is likely. It is therefore suggested that in urban settings CO_2 storage values derived from measurements made at a single height above

Table 2
As Table 1, for $[CO_2]$ time series measured at four heights and interpolated in space. Sample locations (A, E, F, J, Fig. 1d) in brackets indicate the data source for the 'none' interpolation method. The R^2 values are shaded red (poor fit, lower values) to green (better fit, higher values). The RMSE values are shaded green (lower values) to red (higher values). Both R^2 and slope given to 2 d.p., RMSE and intercept to 1 d.p. Also given are the degrees of freedom (DoF).

Interpolation Method	Sample Location	R^2	Intercept (ppm)	Slope	RMSE (ppm)	DoF x10^3
None	B (E)	0.82	64.3	0.84	10.4	41
	C (E)	0.82	50.9	0.87	10.9	41
	D (E)	0.85	50.3	0.87	10.0	41
	G (F)	0.86	3.2	1.00	10.7	38
	H (J)	0.91	28.9	0.93	7.9	38
	I (J)	0.90	30.0	0.93	8.4	38
None	B (A)	0.90	24.0	0.95	7.7	41
	C (A)	0.89	10.5	0.98	8.5	41
	D (A)	0.90	12.5	0.97	7.9	41
	G (F)	0.86	3.2	1.00	10.7	38
	H (J)	0.91	28.9	0.93	7.9	38
	I (J)	0.90	30.0	0.93	8.4	38
Linear	B	0.89	35.2	0.91	8.4	37
	C	0.86	32.2	0.92	9.9	37
	D	0.86	43.9	0.89	9.6	37
	G	0.87	-0.8	1.01	9.9	37
	H	0.94	12.4	0.97	6.2	37
	I	0.91	21.1	0.95	7.8	37
Cubic	B	0.81	76.1	0.81	11.0	37
	C	0.81	61.8	0.84	11.5	37
	D	0.84	57.3	0.86	10.4	37
	G	0.86	10.5	0.98	10.5	37
	H	0.92	25.2	0.95	7.2	37
	I	0.90	26.4	0.94	8.1	37

the canopy cannot be used to correct the vertical flux term for CO_2 stored below the flux measurement height. Despite the relative ease of measurement and calculation of a storage correction term from measurements made at a single height, the data presented here and the analysis of Section 5 discourage its use.

9. Conclusions

CO_2 storage calculated from a switched, time averaged vertical profile (ΔC_{SP}) typically takes values that are smaller than 100th of the magnitude of the vertical flux term and therefore may be considered negligible during well mixed conditions. CO_2 storage calculated from 10 Hz measurements taken at the same height as the flux measurements (ΔC_{SS}) have approximately the same magnitude as the flux measurements. Both are commonly used approaches to evaluating stored carbon dioxide (e.g., Aubinet et al. 2005; Nemitz et al. 2002 for ΔC_{SP} and ΔC_{SS} respectively). Neither fulfil the requirements described in Supplementary material S.2 of continuous CO_2 concentration measurements in time and space, the latter over the vertical extent of the volume of interest. Therefore although both are often assumed to evaluate the same variable (ΔC_S), neither can strictly be said to do so. Whilst this paper does not explicitly discuss which of the two (ΔC_{SP} and ΔC_{SS}) is closer to the 'true' ΔC_S signal, it does evaluate the impact of undersampling in time (relevant to ΔC_{SP}) and space (relevant to ΔC_{SS}). Suggestions for spatial and temporal sampling density of the CO_2 concentration measurements required to calculate CO_2 stored within an urban street canyon, with an empirical correction if the latter cannot be attained, are provided.

Results from London, UK have been reported for a full seasonal cycle and show CO_2 storage to be diurnally and seasonally variable. Approximately 80% of values calculated from a switched profile were within 0 ± 0.13 μmol m^{-2} s^{-1}, of similar magnitude to those reported by studies in tropical and temperate forests. Higher emissions due to traffic and combustion for space heating do not result in larger or more positive CO_2 storage values. The timing of peak ΔC_{SP} is controlled by boundary layer expansion and contraction, and the change in CO_2 concentration with time at each height within the canyon varies more consistently with above canyon wind direction than traffic volume, even at the lowest level. The response to synoptic wind direction suggests the presence of a spiral vortex within the canyon which acts to reduce stored CO_2 on both leeward and windward canyon walls. The observed diurnal and seasonal cycles of ΔC_{SS} were much weaker than for ΔC_{SP}. CO_2 storage calculated from data measured at a single height by LI7500 was one thousand times larger than ΔC_{SP} for the same period; 80% of values were within 0.01–0.11 mmol m^{-2} s^{-1} (i.e., of similar or greater magnitude to observed vertical CO_2 fluxes).

Air within the canyon is well mixed; the vertical CO_2 concentration profile is better approximated by a set of internally homogenous 'zones', rather than a logarithmic decrease with increasing height. For an approximately regular, non-pedestrianised canyon the assumption required for the single-height calculation of CO_2 storage is not valid. However, two heights are sufficient to characterise the profile if placed appropriately with an even spatial distribution. Spatial interpolation of the CO_2 concentration profile was found to be ineffective and unnecessary. Temporally interpolated under-sampled CO_2

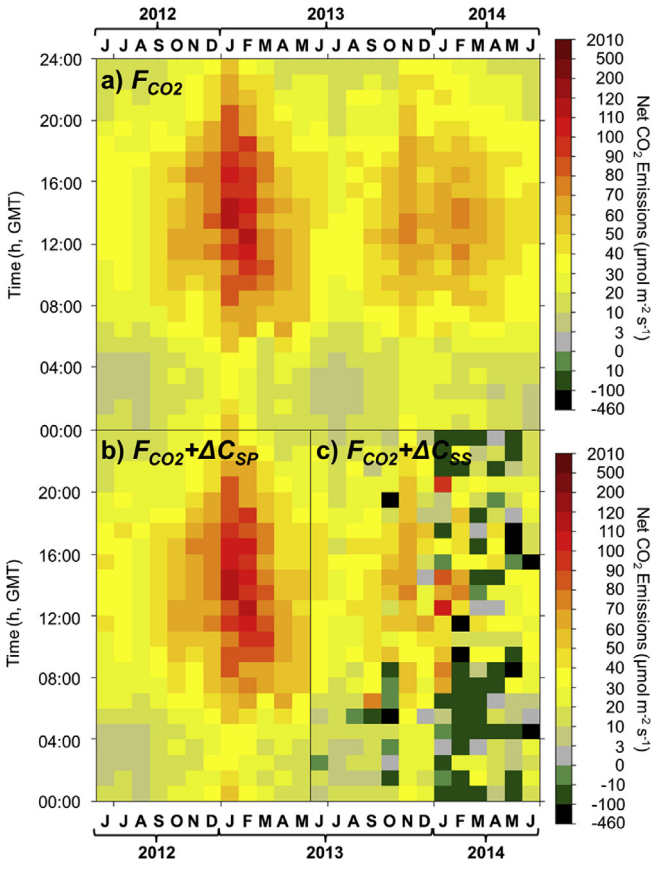

Fig. 14. Net Emissions as calculated from the sum of the vertical CO_2 flux (F_{CO2}) and the CO_2 storage compared to vertical CO_2 flux at KS (London, UK). Diurnal (y-axis) and seasonal (x-axis) cycle of (a) CO_2 vertical flux (key: far right) measured at KSSW, height A (Fig. 1d) for 2012/153–2014/181, (b) CO_2 vertical flux (height A, Fig. 1d) and ΔC_{SP} (heights A – J, switched vertical profile, LI840, Fig. 1d), (c) CO_2 vertical flux (height A, Fig. 1d) and ΔC_{SS} (height A, continuous vertical profile, LI7500, Fig. 1d). All values aggregated by month of year (x-axis) and hour of day (y-axis) in units of μmol m^{-2} s^{-1}. Note: the range of values (a, b) is 3.9 to 120 μmol m^{-2} s^{-1} but are greater for (c).

concentration time series showed very low agreement with a benchmark CO_2 storage time series. It is preferable to have fewer, continuous measurements than a spatially dense switched profile. Under-sampling of the CO_2 concentration time series can lead to an under estimation of CO_2 storage by several orders of magnitude, however this is correctable. CO_2 storage underestimation due to slow sensor response time is not as simple to rectify as the decrease is non-linear. To achieve the recommended response time of 0.1 s or better, fast response/high frequency gas analysers would need to be used.

Previously, both ΔC_{SS} and ΔC_{SP} have been assumed to represent (with some degree of uncertainty) the true ΔC_S signal. The uncertainty in the two measurement methods is in part a function of their underlying assumptions. For example, ΔC_{SS} assumes constant change of CO_2 concentration with time in height such that $\Delta[CO_2]/\Delta t$ is the same at all heights. During periods with strong emissions at ground level, such as rush hour, or periods with weak vertical mixing, the uncertainty in the ΔC_{SS} values increases. Additional uncertainty arises due to insufficient measurement density in space or time, although in this paper the latter (a notable problem with the profile method) has been found to be partially correctable. It is therefore suggested that where possible flux measurements should be corrected by a CO_2 storage term calculated from a vertical profile. If this is not possible then no storage correction should be applied to the vertical flux.

Acknowledgements

This work was made possible by funding to Grimmond as part of the NERC grant NE/H003231/1 ClearfLo project, EU emBRACE (282672), EU BRIDGE (211345) and co-financed by "HORIZON 2020" EU Framework Programme (UrbanFluxes). The numerous individuals who contributed to the installation and maintenance of equipment at King's College London include T. Blackall, B. Main, W. Morrison, L. Pauscher, P. Smith and H. Ward. Special thanks to the KCL Estates team, in particular D. Ede, for their assistance with the tower and knowledge of the Strand building heating system. Additional thanks to E. Nisbet and D. Lowry of Royal Holloway, University of London, for their assistance with the calibration of equipment. Use of trade names does not imply endorsement by the authors or their associated institutions.

Appendix A. Supplementary material

Supplementary material related to this article can be found at http://dx.doi.org/10.1016/j.atmosenv.2015.10.012.

References

Araujo, A.C., Dolman, A.J., Waterloo, M.J., Gash, J.H.C., Kruijt, B., Zanchi, F.B., de Lange, J.M.E., Stoevelaar, R., Manzi, A.O., Nobre, A.D., Lootens, R.N., Backer, J., 2010. The spatial variability of CO_2 storage and the interpretation of eddy covariance fluxes in central Amazonia. Agric. For. Meteorol. 150, 226–237.

Aubinet, M., Heinesch, B., Yernaux, M., 2003. Horizontal and vertical CO_2 advection in a sloping forest. Boundary-Layer Meteorol. 108, 397–417.

Aubinet, M., Berbigier, P., Bernhofer, Ch, Cescatti, A., Feigenwinter, C., Granier, A., Grünwald, Th, Havrankova, K., Heinesch, B., Longdoz, B., Marcolla, B., Montagnani, L., Sedlak, P., 2005. Comparing CO_2 storage and advection conditions at night at different Carboeuroflux sites. Boundary-Layer Meteorol. 116, 63–93.

Baldocchi, D., 2003. Assessing the eddy covariance technique for evaluating carbon dioxide exchange rates of ecosystems: past, present and future. Glob. Change Biol. 9, 479–492.

Canadell, J.G., Ciais, P., Dhakal, S., Le Quéré, C., Patwardhan, A., Raupach, M.R., 2009. The Global Carbon Cycle 2-The Human Perturbation of the Carbon Cycle. UNESCO-SCOPE-UNEP Policy Briefs, No. 10, Paris, France.

Caton, F., Britter, R.E., Dalziel, S., 2003. Dispersion mechanisms in a street canyon. Atmos. Environ. 37, 693–702.

Christen, A., 2014. Atmospheric measurement techniques to quantify greenhouse gas emissions from cities. Urban Clim. 10 (2), 241–260.

Crawford, B., Christen, A., 2014. Spatial variability of carbon dioxide in the urban canopy layer and implications for flux measurements. Atmos. Environ. 98, 302–322.

Department for Transport (DfT), 2013. Table TSGB0106 People Entering Central London During the Morning Peak, Since 1996 (online). https://www.gov.uk/government/statistical-data-sets/tsgb01-modal-comparisons (accessed 09.11.14).

Farge, M., 1992. Wavelet transforms and their applications to turbulence. Annu. Rev. Fluid Mech. 24, 395–445.

Feigenwinter, C., Vogt, R., 2005. Detection and analysis of coherent structures in urban turbulence. Theor. Appl. Climatol. 81 (3–4), 219–230.

Feigenwinter, C., Vogt, R., Christen, A., 2012. Eddy covariance measurements over urban areas. In: Eddy Covariance. Springer, pp. 377–397.

Finnigan, J., 2006. The storage term in eddy flux calculations. Agric. For. Meteorol. 136, 108–113.

Finnigan, J., 2009. Response to comment by Dr. A.S. Kowalski on "The storage term in eddy flux calculations". Agric. For. Meteorol. 149, 725–729.

Greater London Authority (GLA), 2008. The London Plan. Spatial Development Strategy for Greater London. Consolidated with Alterations Since 2004 (online). http://www.london.gov.uk/thelondonplan/thelondonplan.jsp (accessed 09.11.14).

Goulden, M.L., Munger, J.W., Fan, S.-M., Daube, B.C., Wofsy, S.C., 1996. Measurements of carbon sequestration by long-term eddy covariance: methods and a critical evaluation of accuracy. Glob. Change Biol. 2, 169–182.

Grimmond, C.S.B., Oke, T.R., 1999. Heat storage in urban areas: observations and evaluation of a simple model. J. Appl. Meteorol. 38, 922–940.

Grimmond, C.S.B., King, T.S., Cropley, F.D., Nowak, D.J., Souch, C., 2002. Local-scale fluxes of carbon dioxide in urban environments: methodological challenges and results from Chicago. Environ. Pollut. 116 (1), 243–254.

Grimmond, C.S.B., Salmond, J.A., Oke, T.R., Offerle, B., Lemonsu, A., 2004. Flux and turbulence measurements at a densely built-up site in Marseille: heat, mass (water and carbon dioxide), and momentum. J. Geophys. Res. 109. D24101.

Grimmond, C.S.B., Christen, A., 2012. Flux measurements in urban ecosystems. FluxLetter 5 (1), 1–8.

Heinesch, B., Yernaux, M., Aubinet, M., 2007. Some methodological questions concerning advection measurements: a case study. Boundary-Layer Meteorol. 122, 457–478.
Helfter, C., Famulari, D., Phillips, G.J., Barlow, J.F., Wood, C., Grimmond, C.S.B., Nemitz, E., 2011. Controls of carbon dioxide concentrations and fluxes above central London. Atmos. Chem. Phys. 11 (5), 1913–1928.
Hutyra, L.R., Munger, J.W., Hammond Pyle, E., Saleska, S.R., Restrepo-Coupe, Daube, B.C., de Camargo, P.B., Wofsy, S.C., 2008. Resolving systematic errors in estimates of net ecosystem exchange of CO_2 and ecosystem respiration in a tropical forest biome. Agric. For. Meteorol. 148, 1266–1279.
Iamarino, M., Beevers, S., Grimmond, C.S.B., 2012. High-resolution (space, time) anthropogenic heat emissions: London 1970–2025. Int. J. Climatol. 32 (11), 1754–1767.
Iwata, H., Yadvinder, M., van Randow, C., 2005. Gap-filling measurements of carbon dioxide storage in tropical rainforest canopy airspace. Agric. For. Meteorol. 132, 305–314.
Jarvis, P.G., Massheder, J.M., Hale, S.E., Moncrieff, J.B., Rayment, M., Scott, S.L., 1997. Seasonal variation of carbon dioxide, water vapour, and energy exchanges of a boreal black spruce forest. J. Geophys. Res. Atmos. 102 (D24), 28953–28966.
Kotthaus, S., Grimmond, C.S.B., 2012. Identification of micro-scale anthropogenic CO_2, heat and moisture sources – processing eddy covariance fluxes for a dense urban environment. Atmos. Environ. 57, 301–316.
Kotthaus, S., Grimmond, C.S.B., 2014a. Energy exchange in a dense urban environment – Part I: Temporal variability of long-term observations in central London. Urban Clim. 10 (2), 261–280.
Kotthaus, S., Grimmond, C.S.B., 2014b. Energy exchange in a dense urban environment – Part II: Impact of spatial heterogeneity of the surface. Urban Clim. 10 (2), 281–307.
Kowalksi, A.S., 2008. Comment on “the storage term in eddy flux calculations”. Agric. For. Meteorol. 148, 691–692.
Lietzke, B., Vogt, R., 2013. Variability of CO_2 concentrations and fluxes in and above an urban street canyon. Atmos. Environ. 74, 60–72.
Lindberg, F., Grimmond, C.S.B., 2011. Nature of vegetation and building morphology characteristics across a city: Influence on shadow patterns and mean radiant temperatures in London. Urban Ecosyst. 14, 617–634.
Microsoft, Simmons, 2011. Strand Campus, King's College London, UK, 51.511946, -0.116481. (Online). https://www.bing.com/maps/#Y3A9NTIuMjE3NDk5fjAuMTcxNzAwJmx2bD02JnN0eT1yJmVvPTAmcT1XQzJSJTIwMkxT (accessed 14.09.15).
Mölder, M., Lindroth, A., Halldin, S., 2000. Water vapour, CO_2, and temperature profiles in and above a forest—accuracy assessment of an unattended measurement system. J. Atmos. Ocean. Technol. 17, 417–425.
Nemitz, E., Hargreaves, K.J., McDonald, A.G., Dorsey, J.R., Fowler, D., 2002. Micrometeorological measurements of the urban heat budget and CO_2 emissions on a city scale. Environ. Sci. Technol. 36, 3139–3146.
Oke, T.R., 1987. Boundary Layer Climates. Routledge, London.
Press, W.H., Rybicki, G.B., 1988. Fast algorithm for spectral analysis of unevenly sampled data. Astrophys. J. 338, 277–280.
R Development Core Team, 2012. R: A Language and Environment for Statistical Computing. R Foundation for Statistical Computing. Austria, Vienna.
Roth, M., 2000. Review of atmospheric turbulence over cities. Q. J. R. Meteorol. Soc. 126, 941–990.
Salmond, J.A., Oke, T.R., Grimmond, C.S.B., Roberts, S., Offerle, B., 2005. Venting of heat and carbon dioxide from urban canyons at night. J. Appl. Meteorol. 44, 1180–1194.
Satterthwaite, D., 2008. Cities' contribution to global warming: notes on the allocation of greenhouse gas emissions. Environ. Urban. 20 (2), 539–549.
Siebicke, L., Steinfeld, G., Foken, T., 2010. CO_2-gradient measurements using a parallel multi-analyzer setup. Atmos. Meas. Tech. 4 (3), 4383–4421.
Simpson, I.J., Thurtell, G.W., Neumann, H.H., Den Hartog, G., Edwards, G.C., 1998. The validity of similarity theory in the roughness sublayer above forests. Boundary-Layer Meteorol. 87, 69–99.
Torrance, C., Compo, G.P., 1998. A practical guide to wavelet analysis. Bull. Am. Meteorol. Soc. 79 (1), 61–78.
Velasco, E., Roth, M., 2010. Cities as net sources of CO_2: Review of atmospheric CO_2 exchange in urban environments measured by eddy covariance technique. Geogr. Compass 4/9, 1238–1259.
Vogt, R., Christen, A., Rotach, M.W., Roth, M., Satyanarayana, A.N.V., 2006. Temporal dynamics of CO_2 fluxes and profiles over a Central European city. Theor. Appl. Climatol. 84, 117–126.
Ward, H.C., Kotthaus, S., Grimmond, C.S.B., Bjorkegren, A., Wilkinson, M., Morrison, W.T.J., Evans, J.G., Morison, J.I.L., Iamarino, M., 2015. Effects of urban density on carbon dioxide exchanges: Observations of dense urban, suburban and woodland areas of southern England. Environ. Pollut. 198, 186–200.
Wofsy, S.C., Goulden, M.L., Munger, J.W., Fan, S.-M., Bakwin, P.S., Daube, B.C., Bassow, S.L., Bazzazz, F.A., 1993. Net exchange of CO_2 in a mid-latitude forest. Science 260 (5112), 1314–1317.
Xu, L.-K., Matista, A., Hsiao, T.C., 1999. A technique for measuring CO_2 and water vapour profiles within and above plant canopies over short periods. Agric. For. Meteorol. 94, 1–12.
Yang, B., Hanson, P.J., Riggs, J.S., Pallardy, S.G., Heuer, M., Hosman, K.P., Meyers, T.P., Wullschleger, S.D., Gu, L.-H., 2007. Biases of CO_2 storage in eddy flux measurements in a forest pertinent to vertical configurations of a profile system and CO_2 density averaging. J. Geophys. Res. 112, D20.